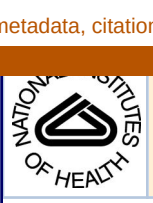

Published in final edited form as:
Nat Biotechnol. 2014 November ; 32(11): 1151–1157. doi:10.1038/nbt.3048.

Differentiation of human pluripotent stem cells to cells similar to cord-blood endothelial colony–forming cells

Nutan Prasain[#1], **Man Ryul Lee**[#2], **Sasidhar Vemula**[1], **Jonathan Luke Meador**[1], **Momoko Yoshimoto**[1], **Michael J Ferkowicz**[1], **Alexa Fett**[1], **Manav Gupta**[1], **Brian M Rapp**[3], **Mohammad Reza Saadatzadeh**[3], **Michael Ginsberg**[4], **Olivier Elemento**[5], **Younghee Lee**[6], **Sherry L Voytik-Harbin**[7], **Hyung Min Chung**[8], **Ki Sung Hong**[9], **Emma Reid**[10], **Christina L O'Neill**[10], **Reinhold J Medina**[10], **Alan W Stitt**[10], **Michael P Murphy**[3], **Shahin Rafii**[4], **Hal E Broxmeyer**[2], and **Mervin C Yoder**[1]

[1]Department of Pediatrics, Indiana University School of Medicine, Indianapolis, Indiana, USA.

[2]Department of Microbiology and Immunology, Indiana University School of Medicine, Indianapolis, Indiana, USA.

[3]Department of Surgery, Indiana University School of Medicine, Indianapolis, Indiana, USA.

[4]Howard Hughes Medical Institute, Weill Cornell Medical College, New York, New York, USA.

[5]Department of Physiology and Biophysics, Weill Cornell Medical College, New York, New York, USA.

[6]Department of Medicine, the University of Chicago, Chicago, Illinois, USA.

[7]Weldon School of Biomedical Engineering, Purdue University, West Lafayette, Indiana, USA.

[8]Kon Kuk University School of Medicine, Seoul, South Korea.

[9]Stem Cell Research Laboratory, CHA University, Seoul, South Korea.

[10]Centre for Experimental Medicine, Queen's University Belfast, Belfast, Northern Ireland, UK.

[#] These authors contributed equally to this work.

Abstract

The ability to differentiate human pluripotent stem cells into endothelial cells with properties of cord-blood endothelial colony–forming cells (CB-ECFCs) may enable the derivation of clinically

Correspondence should be addressed to M.C.Y. (myoder@iu.edu)..

AUTHOR CONTRIBUTIONS

N.P., M.R.L., H.E.B., S.R., M.P.M., A.W.S., S.L.V.-H. and M.C.Y. all participated in the design of the experiments. N.P., M.R.L., S.V., J.L.M., M.Y., M.J.F., A.F., M.G., B.M.R., M.R.S., M.G., O.E., Y.L., H.M.C., K.S.H., E.R., C.L.O. and R.J.M. performed the experiments. N.P. and M.C.Y. wrote the manuscript, and M.R.L., H.E.B., A.W.S., M.G., M.Y., A.F., C.L.O., H.M.C. and K.S.H. provided manuscript edits.

COMPETING FINANCIAL INTERESTS

The authors declare no competing financial interests.

Accession codes. RNA-seq data are deposited into GEO: GSE49074.

Any Supplementary Information and Source Data files are available in the online version of the paper.

relevant numbers of highly proliferative blood vessel–forming cells to restore endothelial function in patients with vascular disease. We describe a protocol to convert human induced pluripotent stem cells (hiPSCs) or embryonic stem cells (hESCs) into cells similar to CB-ECFCs at an efficiency of $>10^8$ ECFCs produced from each starting pluripotent stem cell. The CB-ECFC-like cells display a stable endothelial phenotype with high clonal proliferative potential and the capacity to form human vessels in mice and to repair the ischemic mouse retina and limb, and they lack teratoma formation potential. We identify Neuropilin-1 (NRP-1)-mediated activation of KDR signaling through $VEGF_{165}$ as a critical mechanism for the emergence and maintenance of CB-ECFC-like cells.

ECFCs, also called blood outgrowth endothelial cells[1–3], are rare circulating endothelial cells, particularly abundant in umbilical cord blood, that display robust clonal proliferative potential and intrinsic *in vivo* blood vessel–forming ability[4–7]. ECFCs were shown to engraft in sex-mismatched human bone marrow transplant patients, with the most proliferative ECFCs displaying genetic markings of the donor marrow[1]. Although this study proved that ECFCs are directly transplantable without an intervening period of *in vitro* culture, it did not fully explain the cell of origin within the donor bone marrow that gives rise to ECFCs. ECFCs have shown promise for tissue regeneration. In mouse vascular injury models, they are rapidly recruited to the site of vascular injury or tissue ischemia after intravenous injection, where they initiate a vasculogenic response[8], and they have been reported to enhance vascular repair and improve blood flow after myocardial infarction[9], stroke[3,10], ischemic retinopathy[2] and ischemic limb injury[8,11], and to engraft and re-endothelialize denuded vascular segments or implanted grafts[12]. In elderly patients and subjects with peripheral arterial disease (PAD) and critical limb ischemia, ECFCs may become prone to replicative senescence, reducing their reparative potential. To develop a source of CB-ECFC-like cells for vascular repair, we investigated the use of human pluripotent stem cells (hPSCs)[13,14] , which possess virtually unlimited self-renewal capacity and the ability to differentiate into any cell type in the body.

We began by studying whether previous protocols for generating endothelial cells from hPSCs generate cells with properties of CB-ECFCs, namely, high clonal proliferative potential with self-repopulating activity and robust *in vivo* vessel-forming ability[4,6]. Several of these protocols[15–20] relied on co-culture with OP9 stromal cells[16,20] or embryoid body formation[15,18,19] followed by application of various growth factors and/or receptor signaling pathway inhibitors to promote endothelial cell differentiation. However, the derived endothelial cells are in some cases unstable, drifting to various nonendothelial phenotypes[21], or exhibit low proliferative potential with a tendency to reach replicative senescence within 5–7 passages[18,19,21]. We found that cells derived through co-culture with OP9 cells[16] or through embryoid body formation[15] do not have the specific characteristics of CB-ECFCs (**Supplementary Figs. 1** and **2**).

Next, we tested a more recent two-step endothelial-differentiation protocol that involves initial embryoid body formation and then two-dimensional (2D) adherent cell culture with added growth factors and a TGFβ inhibitor[17] (**Supplementary Fig. 3**). Whereas this paper studied $CD144^+$ cells, we undertook a more directed search for precursors of CB-ECFCs by

looking for other specific markers of endothelial cells in the cultures of differentiating cells. Undifferentiated human pluripotent stem cells express the endothelial marker VEGF receptor 2 (KDR) but not the endothelial markers NRP-1 and CD31. NRP-1 is expressed before CD31, CD34 and CD144 during endothelial line-age differentiation[15] and has a well-established role in cardiovascular development and angiogenesis[22]. Using the protocol of reference 17, we found that only NRP-1$^+$CD31$^+$ cells exhibited high clonal proliferative potential and *in vivo* vessel-forming ability in the continuous presence of TGFβ inhibition during both differentiation and maintenance (**Supplementary Fig. 3**). However, as shown previously[17,21], endothelial cells derived by this protocol became unstable and lost high clonal proliferative potential and *in vivo* vessel-forming ability soon after TGFβ inhibition was removed (data not shown).

To develop a protocol for generating NRP-1$^+$CD31$^+$ cells with CB-ECFC properties that does not require embryoid body formation, co-culture with OP9 cells or TGF-β inhibition, we focused on generating different mesoderm subsets. Human pluripotent cells were cultured in 2D adherent cell culture with added growth factors in a serum-free culture condition (**Fig. 1a**). As Activin-A, BMP-4, FGF-2 and VEGF are critical for the emergence of mesoderm cells and the specification of endothelial cells from mesoderm cells[17,23], we optimized the concentrations of these factors compared with previous protocols. A combination of these factors at a concentration of 10 ng/ml allowed us to enhance and isolate NRP-1$^+$CD31$^+$ cells capable of giving rise to stable CB-ECFC-like cells with clonal proliferative potential and *in vivo* vessel-forming capacity in the absence of TGFβ inhibition.

NRP-1$^+$CD31$^+$ cells gave rise to significantly more endothelial colonies than NRP-1$^-$CD31$^+$ cells ($P < 0.001$; **Fig. 1b**). NRP-1$^+$CD31$^+$ progeny were homogenous and displayed a cobblestone appearance (**Fig. 1**). A significant (15-fold) increase in total cell number was counted in 7-day expansion cultures initiated with NRP-1$^+$CD31$^+$ cells compared to NRP-1$^-$CD31$^+$ cells ($P < 0.001$; **Fig. 1b**). Further, cells grown from the NRP-1$^+$CD31$^+$ fraction exhibited surface co-expression of NRP-1 and CD31 (**Fig. 1d**) and uniform expression of CD144, but lacked expression of the mesenchymal marker α-SMA (**Fig. 1d**). Only 2% of the NRP-1$^+$CD31$^+$ cell subset failed to divide, and 48% formed high proliferative potential–ECFCs (HPP-ECFCs) (defined as single cell–derived colonies with >2,000 progeny that contain self-renewing clonal HPP-ECFC activity) (**Fig. 1e** and **Supplementary Fig. 4e**) with a colony cell number distribution very similar to that of CB-ECFCs (**Fig. 1e**). Furthermore, NRP-1$^+$CD31$^+$ cells formed highly branching capillary structures (**Fig. 1f**). NRP-1$^+$CD31$^+$ cells produced endothelial cells with robust *in vivo* vessel-forming ability; the vessels inosculated with host mouse vessels (**Fig. 1f**,**g**), similar to CB-ECFCs previously described[4,7]. Notably, the NRP-1$^+$CD31$^+$ cells did not form teratomas after >6 months of implantation into immunodeficient mice ($n = 24$ animals; data not shown). Thus, hESC- and hiPSC-derived NRP-1$^+$CD31$^+$ cells displayed properties of ECFCs similar to CB-ECFCs and will be referred to hereafter as hESC-ECFCs or hiPSC-ECFCs or, when discussing results derived from both, hPSC-ECFCs. hPSC-derived NRP-1$^-$CD31$^+$ cells did not show these properties (**Supplementary Fig. 4**).

We used two additional models to test the endothelial function of hiPSC-ECFCs, in addition to our subcutaneous implant method. We compared three study groups: (i) hiPSC-ECFCs,

(ii) hiPSC-embryoid body-derived TGFβ-inhibited $CD144^+$ endothelial cells (hiPSC- EBT-$CD144^+$ ECs)[17] and (iii) CB-ECFCs[4,6]. Although we sought to test a fourth study group, we were unable to derive enough hiPSC-embryoid body-derived $KDR^+NRP\text{-}1^+$ endothelial cells to perform these comparative studies.

In the first model, we measured rescue of blood vessel formation and reduction of neovascular tufts in newborn mice exposed to high oxygen concentration[2]. The oxygen-induced retinopathy (OIR) in the neonatal pups results from hypoxia-induced loss of retinal vessels followed by an overexuberant retinal hypoxic response. A significant reduction of the post-injury avascular area occurred in retinas that received hiPSC-ECFCs (≥36% reduction; $^{**}P < 0.01$) but not in retinas that received hiPSC-EBT-$CD144^+$ ECs (≤14% reduction in avascular area; P = not significant (ns)) (**Fig. 2a,b**). In addition, only hiPSCECFCs significantly reduced preretinal neovascular tufts (**Fig. 2c**; hiPSC-EBT-$CD144^+$ EC results not shown). Prelabeling of the cells with Qdots 655 and imaging at 72 h after cell delivery showed that hiPSC-ECFCs integrated in higher numbers and with wider distribution in host retinal tissue compared with hiPSC-EBT-$CD144^+$ ECs (**Supplementary Fig. 5a**). The hiPSC-ECFCs but not the hiPSC-EBT$CD144^+$ ECs also appeared to form vascular tube structures in the superficial retinal plexus (**Supplementary Fig. 5b**).

We also studied a model of hind limb femoral vessel removal in nude mice[24]. Salvage of ischemic limbs and blood flow were significantly improved by hiPSC-ECFCs compared with hiPSC- EBT-$CD144^+$ ECs ($P < 0.05$; **Fig. 2d–f** and data not shown). In these assays, hiPSC-ECFCs functioned similarly to CB-ECFCs.

Primary cells do not proliferate indefinitely but instead undergo senescence after long-term *in vitro* culture[25]. We could expand both hPSC-ECFCs and CB-ECFCs up to passage 18 (P18) without loss of typical endothelial cell features (**Supplementary Fig. 6a–c**). Notably, although the majority of P18 hPSC-ECFCs and CB-ECFCs were senescent and exhibited characteristics of mortal primary cells[25], they still maintained an endothelial cobblestone morphology and expression of endothelial antigens CD31, NRP-1 and CD144, but not α-SMA (**Supplementary Fig. 6d**). Thus, hPSC-ECFCs maintained a stable endothelial phenotype throughout long-term expansion culture but, like any primary cell type, eventually exhibited replicative senescence.

To compare the various ECFC subsets at the transcriptional level, we performed whole-transcriptome sequencing (RNA-seq) analysis on undifferentiated hiPSCs (hiPSC-day 0), day 3 differentiated hiPSCs (hiPSC-day 3), day 12 hiPSC-ECFCs, day 12 hESC-ECFCs and CB-ECFCs, as previously described[21]. Notably, both hiPSC- and hESC-ECFCs exhibited decreased expression of pluripotent and nonendothelial lineage–specific gene transcripts but increased expression of endothelial gene transcripts (**Supplementary Fig. 7a,b**), similar to CB-ECFCs.

We investigated an approach for enhancing the generation of hPSC-ECFCs. KDR has a well-established role in endothelial specification and maintenance, but it is unknown whether NRP-1 enhances KDR activation in hiPSCs undergoing ECFC lineage differentiation and increases the generation of stable ECFCs. It has been proposed that

NRP-1 on the endothelial cell surface binds to $VEGF_{165}$ as a co-receptor with KDR[22]. Formation of NRP-1-$VEGF_{165}$-KDR signaling complexes enhances VEGF-KDR-mediated signaling activity and biological function[22,26,27]. NRP-1 has also been clearly shown to be required for maximum KDR activity and/or KDR tyrosine phosphorylation[22,26,27,] and to selectively mediate VEGF-KDR signaling through $p130^{Cas}$/Pyk2 activation in endothelial cells[22]. To study whether increasing NRP-1 activity would enhance KDR activation and the generation of hPSC-ECFCs, we screened for and identified the mesoderm subset with robust KDR expression and the first evidence of NRP-1 expression, which emerged on day 6 of hPSC differentiation (inset, **Fig. 3b**). We modulated NRP-1 expression in these cells with dimeric Fc-NRP-1, a surrogate for membrane NRP-1 (ref. 28), which enhances NRP-1 activity, or the monoclonal antibody, NRP-1-B[27], which blocks NRP-1 activity. Dose-response experiments identified a specific dose (3.3 nM for Fc-NRP-1 dimer and 500 ng/ml for NRP-1-B) and length of time (4–6 d) for the treatment that gave reproducible results (data not shown and **Fig. 3a**) as reported[27,28]. After 4 d of treatment, Fc-NRP-1 dimer significantly increased ($P < 0.01$) and NRP-1-B significantly diminished ($P < 0.001$) generation of $NRP\text{-}1^{+}CD31^{+}$ cells (**Fig. 3b**). Fc-NRP-1 dimer treatment also increased activation of KDR and of $p130^{Cas}$, a downstream molecule activated by NRP-1-mediated activation of KDR[22] (**Fig. 3c** and **Supplementary Fig. 8**). In contrast, NRP-1-B–treated cells displayed decreased KDR phosphorylation and reduced activation of downstream molecules (**Fig. 3c** and **Supplementary Fig. 8**). These data suggest that NRP-1 enhanced the generation of ECFCs from human pluripotent stem cells by potentiating KDR signaling.

Next, we asked whether NRP-1 is also involved in the maintenance of the proliferative potential of cultured ECFCs. NRP-1 expression was progressively downregulated in late-passage hPSC-ECFCs, and low levels of NRP-1 expression in late ECFCs were associated with decreased total proliferative potential (**Fig. 4a,b**). In late-passage (P14) hPSC-ECFCs, KDR was expressed in 50–60% of cells (**Fig. 4c**). However, when cultured in the presence of Fc-NRP-1 for 7 d, P14 hPSC-ECFCs displayed significantly increased ($P < 0.001$) expansion (**Fig. 4d**) but decreased β-galactosidase expression (senescence marker) compared to control and NRP-1-B–treated groups (**Fig. 4e,f**). Fc-NRP-1–treated P14 hPSC-ECFCs also displayed a significant decrease in the percentage of pro-apoptotic cells compared to control treated ($P < 0.01$) cells (**Fig. 4g**). Furthermore, the effects of Fc-NRP-1 on KDR activation were dependent upon the presence of $VEGF_{165}$, as $VEGF_{121}$ did not promote interaction between Fc-NRP-1 and KDR-positive P14 hPSC-ECFC (**Fig. 4g–i**). Thus, Fc-NRP-1 activation of KDR by $VEGF_{165}$ contributes to the rescue of proliferation and the reduction of expression of senescence markers and of pro-apoptotic behavior in near-senescent hPSC-ECFCs.

Finally, preliminary studies showed that circulating and resident arterial-derived primary endothelial cells derived from patients with PAD and critical limb ischemia exhibited low levels of NRP-1 expression, possessed low clonal proliferative potential, exhibited markers of senescence and did not form robust *in vivo* human vessels upon implantation in immunodeficient mice (**Supplementary Fig. 9a–g**). However, Fc-NRP-1 treatment facilitated proliferation, survival and modestly diminished evidence of senescence in these cells (**Supplementary Fig. 9h–n**). Thus, Fc-NRP-1 treatment of late-passage, near-

senescent hiPSC-ECFCs and patient-derived PAD-ECs increases proliferative potential, decreases apoptosis and diminishes markers of senescence in a $VEGF_{165}$-dependent fashion.

In this study we have established a method to reproducibly derive and isolate a homogenous and stable population of pluripotent stem cell–derived endothelial cells possessing CB-ECFC properties: formation of a homogenous monolayer with characteristic cobblestone appearance, high clonal proliferative potential, formation of capillary structures when cultured on Matrigel and generation of robust *in vivo*-inosculated vessels after implantation in immune-deficient mice. By assaying for specific CB-ECFC properties rather than simply relying on classical cell surface expression of 'endothelial' markers or gene expression patterns, we derived ECFCs that we did not detect among the endothelial cells derived by previous methods[15–17]. The hiPSC-ECFCs significantly contributed to vascular repair of experimentally induced ischemic limbs and hyperoxic injured retinas in murine models, similar to CB-ECFCs, and were superior to endothelial cells isolated using other published protocols[15–17]. They were stable and did not transition to nonendothelial cells over prolonged culture (18 passages) and could expand to over a trillion endothelial cells in less than 3 months (**Fig. 1a**). This efficient output of functional endothelial cells contrasts with previous reported yields of 0.6 (ref. 16), 7.4 (ref. 17) and 11.6 (ref. 29) endothelial cells from differentiated human pluripotent stem cells. We also found that NRP-1-$VEGF_{165}$-KDR–mediated activation of KDR is a critical mechanism both for derivation of hPSC-ECFCs and for enhancing survival and proliferative potential of late-passage, near-senescent hPSC-ECFCs and patient-derived ECFCs. Our results may enable highly efficient production of patient-derived ECFCs for the treatment of cardiovascular disease.

ONLINE METHODS

Culturing of hESCs and hiPSC

hESC line H9 (ref. 13) and fibroblast-derived human iPSC line (DF19-9-11T)[14] were purchased from WiCell Research institute (Madison, Wisconsin). Several other hiPSC lines (FCB-iPS-1 and FCB-iPS-2) derived in the Broxmeyer and Yoder laboratories were also used to generate ECFCs[30,31] (**Supplementary Table 1**). Both hESCs and hiPSCs were maintained in mTeSR1 complete media (Stem Cell Technologies) on Matrigel in 10 cm^2 tissue culture dishes at 37 °C and 5% CO_2. After the plating of cells, media was changed on days 2, 3 and 4. Cells were passaged on day 5. Media was aspirated and 4–5 ml of dispase (2 mg/ml, Gibco) containing media was added to the plate and incubated at 37 °C for 3–5 min or until the edges of the colonies had lifted from the plate. Dispase containing media was aspirated from the plate and cells were gently washed with DMEM-F12 (Gibco) three times to remove any residual amount of enzyme. Fresh media was then used to collect colonies from the plate using a forceful wash and scraping with a 5-ml disposable pipette taking care to avoid bubbles. Collected colonies were then centrifuged at 300 *g* for 5 min. The supernatant was aspirated and pellet was resuspended in mTeSR1 complete media. Prior to passaging, 10 cm^2 tissue culture dishes were coated with Matrigel for 30 min. Unattached Matrigel was removed from the tissue culture dishes and 7 ml of mTeSR1 complete medium was added to dishes. Colonies evenly distributed in mTeSR1 media were added to each plate. Cells were then spread out within the dish using multiple side-to-side shaking motions

while avoiding any swirling. Cultures were checked for growth quality and morphology, and by performing teratoma formation assay as previously described[31].

Directed differentiation of hESCs and hiPSCs into the ECFC lineage

After 2 d (-D2) of culture in mTeSR1 media, cultures were directed toward the mesodermal lineage with addition of activin A (10 ng/ml) in the presence of FGF-2, $VEGF_{165}$ and BMP4 (10 ng/ml) for 24 h. The following day, activin-A containing media was removed and replaced with 8 ml of Stemline II complete media (Sigma) containing FGF-2 (Stemgent), $VEGF_{165}$ (R&D) and BMP4 (R&D) to promote endothelial cell emergence and expansion. Media was replaced with 8 ml of fresh Stemline II differentiation media on days 3, 5, 7 and 8. On day 9 and thereafter media was changed with 10 ml of Stemline II differentiation media.

Flow cytometry

At day 12 after differentiation, adherent cells were harvested using TrypleE and made into a single-cell suspension in EGM-2 medium. Cells were counted and aliquots of the cell suspension were prepared for antibody staining. FcR blocking reagent (Miltenyi Biotech) was added to prevent the non-specific binding of antibodies. Anti-human CD31 (CD31-FITC, clone WM59 from BD Pharmingen), CD144 (CD144-PE, clone 16B1 from eBioscience) and NRP-1 (NRP-1-APC, clone AD5-176 from Miltenyi Biotech) antibodies were used at concentrations that were titrated before use (**Supplementary Table 2**). Propidium iodide (PI, Sigma) was added to the cell suspension for dead cell staining. Flow cytometric detection of the cell surface antigens and cells sorting were performed on an LSR II and FACSAria (Becton Dickinson), respectively. Compensation was set by single-positive controls using cord blood–derived ECFCs. A gating of targeted cell population was determined based on fluorescent minus one (FMO) controls for each fluorescent color.

Cell culture of sorted cells

$CD31^+$-, $CD144^+$- or KDR^+- and $NRP\text{-}1^+$–sorted cells were centrifuged at 300 *g* for 5 min then resuspended in 50% EGM-2 and 50% complete Stemline II differentiation media. To generate ECFCs from the sorted population, 2,500 cells per well were seeded on rat tail type I collagen-coated 12-well plates. After 2 d, the media was aspirated and three parts of EGM-2 and one part of differentiation media was added to the cultures. ECFC colonies appeared as tightly adherent cells and exhibited cobblestone morphology on day 7. On occasion, cloning cylinders were used to isolate ECFC colonies from heterogeneous cell populations. Cloning of endothelial cell clusters was performed to isolate pure populations of highly proliferative endothelial cells as described previously[4,5]. Confluent ECFCs were passaged by plating 10,000 cells per cm^2 as a seeding density and ECFCs were maintained in complete endothelial growth media (collagen coated plates and cEGM-2 media) with media change every other day as described previously[4,5].

In vitro capillary network formation assay on Matrigel

Endothelial cells derived from different protocols were trypsinized and resuspended in EGM-2 media. Cells were plated at a density of 1.0×10^4 cells per well in triplicate in 96-

well plates coated with 50 μl of growth factor–reduced Matrigel (BD Biosciences). Plates were incubated overnight at 37 °C. After 8–16 h of incubation, photomicrographs were taken from each well at 10× magnification using a Zeiss Axiovert 25 CFL inverted microscope with a 10× CP-ACHROMAT/0.12 NA objective. Images were acquired using a SPOT RT color camera (Diagnostic Instruments) with the manufacturer's software. Phase contrast images were taken with air objectives.

Immunochemistry

ECFCs were fixed with 4% (w/v) paraformaldehyde for 30 min and permeabilized with 0.1% (v/v) Triton X-100 in PBS for 5 min. After blocking with 10% (v/v) goat serum for 30 min, cells were incubated with primary following antibodies; anti-CD31 (Santa Cruz), anti-CD144 (Ebioscience), anti-NRP-1 (Santa Cruz) and anti-a-SMA, (Chemicon) overnight at 4 °C. Cells were washed with PBS, then incubated with secondary antibodies conjugated with Alexa-488 or Alexa-565 (Molecular Probe) and visualized by confocal microscopy after counterstaining with 2 g/ml DAPI (Sigma-Aldrich). The confocal images were obtained with an Olympus FV1000 mpE confocal microscope using as an Olympus uplanSApo 60xW/1.2NA/eus objective. All the images were taken as Z-stacks with individual 10-μm thick sections at room temperature and images were analyzed using FV10-ASW 3.0 Viewer.

Single-cell assay

CB-ECFCs or iPSC-ECFCs or hESC-ECFCs or hiPSCEBT-CD144^{+} ECs and PAD-derived ECs were subjected to a single-cell assay to evaluate clonogenic proliferative potential. Briefly, endothelial cells were treated with trypLE Express (Invitrogen) to obtain a single-cell suspension. Cell counts and serial dilutions were performed to obtain a concentration of 0.68 cells per well in individual wells of 96-well culture plates. Wells were examined the day after plating to ensure the presence of a single cell per well. Culture media was changed on days 4, 8 and 12. On day 14 of culture, cells were stained with Sytox reagent (Invitrogen), and each well was examined to quantitate the number of cells using a fluorescent microscope. Those wells containing two or more cells were identified as positive for proliferation under a fluorescent microscope at 10× magnification using a Zeiss Axiovert 25 CFL inverted microscope with a 10 × CP-ACHROMAT/0.12 NA objective. Wells with endothelial cell counts of 2–50, 51–500, 501–2,000 and ≥2,001 were labeled as endothelial cell clusters (ECCs), low proliferative potential ECFCs (LPP) and high proliferative potential ECFCs (HPP), as previously described[4,5].

Cell viability, senescence and cell proliferation assay

Endothelial cells were plated at a density of 5×10^4 per well or 1×10^5 per well on type I collagen–coated 12-well and 6-well plates, respectively. After 24 h, growth media was replaced with Fc-control, Fc-NRP-1 dimer (R&D Systems) or NRP-1 blocking antibodies containing EGM-2 medium for 7 d and media was replaced on every alternative day. NRP-1A and NRP-1B antibodies were generously provided by Genentech[27]. Cell viability and proliferation was assessed by Trypan blue exclusion, and the numbers of dye-free cells were counted under a phase microscope in triplicate per condition.

A senescence assay kit was purchased from Biovision, and the assay performed according to the manufacturer's instructions. Briefly, endothelial cells were seeded onto 12-well plates for overnight culture to form a monolayer. The following day, cells were fixed in 0.5 ml of the commercial fixative solution for 10–15 min at room temperature. Cells were washed twice with 1 ml of 1× PBS and stained with 0.5 ml of the commercial staining solution for overnight at 37 °C. Cells were observed under a microscope for development of a blue color. Photomicrographs were taken from each well at 10× magnification using a Zeiss Axiovert 25 CFL inverted microscope with a 10× CP-ACHROMAT/0.12 NA objective. Images were acquired using a SPOT RT color camera (Diagnostic Instruments) with the manufacturer's software. Phase contrast images were taken with air objectives.

Mice

All animal procedures were carried in accordance with the Guidelines for the Care and Use of Laboratory Animals and were approved by the Institutional Animal Care and Use Committees (IACUCs) at Indiana University School of Medicine (IACUC protocol # 10170). Both male and female 6- to 12-week-old nonobese/severe combined immunodeficient (NOD/SCID) mice (T- and B-cell deficient, impaired complement) were used for all animal studies. NODSCID mice were maintained under specific-pathogen-free conditions at the Indiana University Laboratory Animal Resource Center (LARC). Previous work with this animal model was used to determine the minimum number of animals needed to obtain statistically significant results[4]. Previous studies have shown that 8 out of 10 matrices (one animal received two matrices) implanted inosculate with the host vasculature and that 8 matrices (4 animals) with functional vessels are needed for each group for statistical significance[4]. Method of randomization was not used while allocating samples and animals to each experimental group. Also, investigator was not blinded to the group allocation either during the experiment or when accessing the outcomes.

In vivo vessel formation assay

Pig skin type I collagen was used to generate three-dimensional (3D) cellularized collagen matrices as previously described[7]. Briefly, type 1 collagen gel mixture was prepared by mixing together ice-cold porcine skin collagen solution in 0.01N HCL, and neutralized with phosphate buffered saline and 0.1N NaOH to achieve neutral pH (7.4). Neutralized gel mixtures (~1.5 mg/ml) were kept on ice before induction of polymerization by warming at 37 °C, in 5% CO_2. Cultured ECFCs were added to the collagen mixture to a final concentration of two million cells/ml collagen. The collagen mixture (250 μl) containing the ECFCs suspension was added to 48-well tissue culture dishes and was allowed to polymerize to form gels by incubation in a CO_2 incubator at 37 °C for 30 min. The gels were then overlaid with 500 μl of culture medium for overnight at 37 °C, in 5% CO_2.

After 18 h of *ex vivo* culture, cellularized gels were implanted into the flanks (a bluntly dissected subcutaneous pouch of anterior abdominal wall with close proximity of host vasculature) of 6- to 12-week-old NOD/SCID mice, as previously described[4]. Surgical procedures to implant collagen gels were conducted under anesthesia and constant supply of oxygen. Incisions were sutured and mice monitored for recovery. Two weeks after implantation, gels were recovered by excising engrafts in animals that had been humanely

euthanized per approved IACUC protocol. Immunohistochemistry was performed as described previously using H&E and anti-human CD31 staining to examine the gels for human endothelial-lined vessels perfused with mouse red blood cells. $hCD31^+$ blood vessels were imaged from each explant using a Leica DM 4000B microscope (Leica Microsystems) with attached Spot-KE digital camera (Diagnostic Instruments). Functional vessels were counted only if they contained at least 1 mouse erythrocyte.

Oxygen-induced retinopathy model

All experiments were performed in conformity to the ARVO Statement for the Use of Animals in Ophthalmic and Vision Research and the UK Home Office Regulations. Oxygen-induced retinopathy was induced in C57/BL6 wild-type mice, as previously described[2]. Briefly, postnatal day (P) 7 newborn mice and their nursing dams were exposed to 75% oxygen (Pro-Ox 110 Chamber Controller; Biospherix, Redfield, NY) for 5 d. At P12 they were transferred back to room air. At P13, mice received a 1 μl intravitreal injection containing 1×10^5 hiPSC-ECFCs, hiPSC-EBT-$CD144^+$ ECs or CB-ECFCs that had previously been labeled (Qtracker 655; Invitrogen). Phenol red–free DMEM without growth factors and serum was used as vehicle and injected in the left eye of each pup as a control. All pups were euthanized 72 h later with sodium pentobarbital and eyes fixed in 4% paraformaldehyde. Retinal flat mounts were stained with isolectin B4 (Sigma) and streptavidin-AlexaFlour488 (Invitrogen), and stained retinas were visualized and imaged using a confocal microscope. Area quantification was performed using ImageJ software by three independent, blinded investigators as described[2].

Mouse hind limb ischemia model

Hind limb ischemia experiments were performed as we previously described[24]. Briefly, 6-week-old male athymic nude mice (body weight 25–30 g; Orient bioAnimal Inc., Seoul, Korea) were anesthetized with rompun (20 mg/kg) and ketamine (100 mg/kg). The femoral artery and its branches were ligated through a skin incision with 6-0 silk (Ethicon). The external iliac artery and all of the arteries above it were then ligated. The femoral artery was excised from its proximal origin as a branch of the external iliac artery to the distal point where it bifurcates into the saphenous and popliteal arteries. Immediately after arterial dissection, athymic mice were randomly assigned to 1 of 4 experimental groups. After the ischemic surgery, the hiPSC-ECFCs or CB-ECFCs or hiPS-EBT-$CD144^+$ ECs (1.0×10^6 cells per mouse) were suspended in 200 μl of EGM-2 and these cells or vehicle control were injected intramuscularly into six sites of the gracilis muscle in the medial thigh with 29-gauge tuberculin syringes. A Laser Doppler perfusion imager (Moor Instruments) was used to measure the blood flow in the hind limbs on days 0 and 28 post-treatment as previously described[24]. Digital color-coded images were analyzed to quantify the blood flow in the region from the knee joint to the toe, and the mean perfusion values were calculated. All animal care and experimental procedures for hind limb ischemia experiments were performed under the approval of the animal care committees of CHA University (IACUC No. 130024).

Isolation of arterial ECFCs from patients with peripheral vascular disease (PAD)

De-identified patient materials (Disease artery (DA) ECFCs) were obtained from patients with peripheral vascular disease who underwent lower extremity amputations following informed consent and use of a protocol that was approved by the Indiana University and the Richard L. Roudebush VA Medical Center human IRB panel (IRB # 1011004004). Patients with active cellulitis, purulent drainage or wet gangrene were not used in this study, due to the high risk of yeast contamination. Likewise, patients with hepatitis B or C, and patients with HIV were excluded from this study. Following transection, amputated legs were immediately explored in the operating room for suitable specimens of arteries on a sterile table separate from the operative field. Samples deemed suitable were placed into a container filled with Hank's balanced salt solution (HBSS; Invitrogen) and taken to the laboratory for processing. Under sterile conditions, the vessels were opened lengthwise in a tissue culture dish and immersed in EGM-2 culture media (Lonza). The intima of each vessel was scraped with a cell scraper (TPP) and washed with DMEM. The cell fraction left from the washings was centrifuged at 1620 r.p.m. for 10 min, after which it was plated onto rat-tail type I collagen coated six-well plates. After several days, growing endothelial colonies could be seen by light microscopy, and these colonies were isolated with cloning cylinders, trypsinized and replated onto new six-well plates to prevent mesenchymal cell contamination. The purified ECFCs were passaged 1 to 2 times more, and then expanded in T-75 tissue culture flasks (TPP) before cryopreservation.

Culture of endothelial cells from peripheral blood of PAD patient

Mononuclear cells isolated from each patient peripheral blood or cord blood were seeded on 6-well tissue culture plate precoated with type I rat tail collagen and were cultured in complete endothelial growth medium (EGM-2) supplemented with 10% FBS, 2% penicillin-streptomycin. Cells were maintained in a 37 °C, 5% CO_2 humidified incubator, and medium was changed every other day for 2–3 weeks or until cobblestone-appearing endothelial colonies appeared. After initial appearance of colonies, cells were transferred to a new well of a 6-well plate and further passaged in 25-cm^2 flasks and at passages at 85–95% confluence. PAD cells at passages 3–7 at approximately 70% confluence were used in all studies.

Western blot analysis

Cell lysates were prepared by resuspending cells in lysis buffer (20 mM Tris-HCl pH 7.5, 150 mM NaCl, 10% glycerol, 1% Triton X-100, 2 mM EDTA, 1 mM Na_3VO_4, 1 μg/ml each of aprotinin and leupeptin) followed by incubation on ice for 20 min. Insoluble components were removed by centrifugation at 12,000*g* for 15 min. Protein concentrations were determined with a protein assay kit (Bio-Rad). Proteins were separated by electrophoresis on 4–20%Tris-glycine minigels and then transferred onto immobilon-FL PVDF membrane (Millipore). Nonspecific binding was blocked with blocking buffer for 1 h at room temperature and incubated overnight at 4 °C with primary antibodies against phospho-PYK2 (1:1,000; Cell Signaling) and phospho-$p130^{Cas}$ (1:1,000; Cell Signaling) in Odyssey blocking buffer. Blots were washed with PBS containing 0.1% Tween20, followed by

incubation for 1 h at room temperature with anti-rabbit antibody (1:10,000; LI-COR). Immunoreactive bands were detected using the Odyssey Infrared Imager (LI-COR).

RNA sequence library construction, sequencing and analysis

Total RNA was isolated from the samples using Trizol reagent (Invitrogen) and the RNA quality was examined as previously described[21]. RNA sequence library was generated using 1 μg of high-quality total RNA and sequencing was performed using Illumina HiSeq2000 sequencer as previously described[21]. The resulting sequence reads were mapped to the human genome (hg18) using TopHat with default parameters, and the RefSeq (June 2010) transcript levels (FPKMs) were quantified using CuffLinks. Heatmaps of select transcripts were then plotted using red-to-green scale using R statistical software package of heatmap.2 from RNA-seq data.

Statistical analysis

All experiments were performed ≥3 times in triplicate and data are represented as mean value ± s.d. for statistical comparison. A power of analysis with a 95% confidence interval was used to calculate sample size required to obtain statistically significant results. The sampling number we used gave a normal distribution. Significance of differences was assessed by a two-tailed Student's *t*-test or one way ANOVA-Tukey post-hoc test Multiple Comparison Test or chi-squared test.

Supplementary Material

Refer to Web version on PubMed Central for supplementary material.

ACKNOWLEDGMENTS

These studies were supported by funds provided by the Riley Children's Foundation (M.C.Y.), by an AHA postdoctoral fellowship (N.P.), and Public Health Service Grants R01 HL109602 (M.C.Y. and S.L.V.-H.), RO1 HL056416 (H.E.B.), RO1 HL067384 (H.E.B.), PO1 DK090948 (H.E.B. and M.C.Y.), and by the Bio & Medical Technology Development Program of the National Research Foundation (NRF), which is funded by the South Korean government (MEST; No. 2011-0019487). The authors thank H.P. Poudel (Indiana University Purdue University Indianapolis) for critical input in biostatistical analysis. The authors also thank H.J. Lee (CHA Stem Cell Institute, CHA University, South Korea) for HLI experiments.

References

1. Lin Y, Weisdorf DJ, Solovey A, Hebbel RP. Origins of circulating endothelial cells and endothelial outgrowth from blood. J. Clin. Invest. 2000; 105:71–77. [PubMed: 10619863]
2. Medina RJ, O'Neill CL, Humphreys MW, Gardiner TA, Stitt AW. Outgrowth endothelial cells: characterization and their potential for reversing ischemic retinopathy. Invest. Ophthalmol. Vis. Sci. 2010; 51:5906–5913. [PubMed: 20554606]
3. Moubarik C, et al. Transplanted late outgrowth endothelial progenitor cells as cell therapy product for stroke. Stem Cell Rev. 2011; 7:208–220. [PubMed: 20526754]
4. Yoder MC, et al. Redefining endothelial progenitor cells via clonal analysis and hematopoietic stem/progenitor cell principals. Blood. 2007; 109:1801–1809. [PubMed: 17053059]
5. Ingram DA, et al. Vessel wall-derived endothelial cells rapidly proliferate because they contain a complete hierarchy of endothelial progenitor cells. Blood. 2005; 105:2783–2786. [PubMed: 15585655]

6. Ingram DA, et al. Identification of a novel hierarchy of endothelial progenitor cells using human peripheral and umbilical cord blood. Blood. 2004; 104:2752–2760. [PubMed: 15226175]
7. Critser PJ, Kreger ST, Voytik-Harbin SL, Yoder MC. Collagen matrix physical properties modulate endothelial colony forming cell-derived vessels in vivo. Microvasc. Res. 2010; 80:23–30. [PubMed: 20219180]
8. Schwarz TM, et al. Vascular incorporation of endothelial colony-forming cells is essential for functional recovery of murine ischemic tissue following cell therapy. Arterioscler. Thromb. Vasc. Biol. 2012; 32:e13–e21. [PubMed: 22199368]
9. Kang KT, Coggins M, Xiao C, Rosenzweig A, Bischoff J. Human vasculogenic cells form functional blood vessels and mitigate adverse remodeling after ischemia reperfusion injury in rats. Angiogenesis. 2013; 16:773–784. [PubMed: 23666122]
10. Huang XT, et al. Intracerebroventricular transplantation of ex vivo expanded endothelial colony-forming cells restores blood-brain barrier integrity and promotes angiogenesis of mice with traumatic brain injury. J. Neurotrauma. 2013; 30:2080–2088. [PubMed: 23957220]
11. Heo SC, et al. WKYMVm-induced activation of formyl peptide receptor 2 stimulates ischemic neovasculogenesis by promoting homing of endothelial colony forming cells. Stem Cells. 2013; 32:779–790. [PubMed: 24155208]
12. Stroncek JD, Ren LC, Klitzman B, Reichert WM. Patient-derived endothelial progenitor cells improve vascular graft patency in a rodent model. Acta Biomater. 2012; 8:201–208. [PubMed: 21945828]
13. Thomson JA, et al. Embryonic stem cell lines derived from human blastocysts. Science. 1998; 282:1145–1147. [PubMed: 9804556]
14. Yu J, et al. Human induced pluripotent stem cells free of vector and transgene sequences. Science. 2009; 324:797–801. [PubMed: 19325077]
15. Cimato T, et al. Neuropilin-1 identifies endothelial precursors in human and murine embryonic stem cells before CD34 expression. Circulation. 2009; 119:2170–2178. [PubMed: 19364973]
16. Choi KD, et al. Hematopoietic and endothelial differentiation of human induced pluripotent stem cells. Stem Cells. 2009; 27:559–567. [PubMed: 19259936]
17. James D, et al. Expansion and maintenance of human embryonic stem cell-derived endothelial cells by TGFbeta inhibition is Id1 dependent. Nat. Biotechnol. 2010; 28:161–166. [PubMed: 20081865]
18. Goldman O, et al. A boost of BMP4 accelerates the commitment of human embryonic stem cells to the endothelial lineage. Stem Cells. 2009; 27:1750–1759. [PubMed: 19544443]
19. Feng Q, et al. Hemangioblastic derivatives from human induced pluripotent stem cells exhibit limited expansion and early senescence. Stem Cells. 2010; 28:704–712. [PubMed: 20155819]
20. Sone M, et al. Pathway for differentiation of human embryonic stem cells to vascular cell components and their potential for vascular regeneration. Arterioscler. Thromb. Vasc. Biol. 2007; 27:2127–2134. [PubMed: 17872458]
21. Ginsberg M, et al. Efficient direct reprogramming of mature amniotic cells into endothelial cells by ETS factors and TGFbeta suppression. Cell. 2012; 151:559–575. [PubMed: 23084400]
22. Zachary IC. How neuropilin-1 regulates receptor tyrosine kinase signalling: the knowns and known unknowns. Biochem. Soc. Trans. 2011; 39:1583–1591. [PubMed: 22103491]
23. Evseenko D, et al. Mapping the first stages of mesoderm commitment during differentiation of human embryonic stem cells. Proc. Natl. Acad. Sci. USA. 2010; 107:13742–13747. [PubMed: 20643952]
24. Cho SW, et al. Improvement of postnatal neovascularization by human embryonic stem cell derived endothelial-like cell transplantation in a mouse model of hindlimb ischemia. Circulation. 2007; 116:2409–2419. [PubMed: 17984381]
25. Kuilman T, Michaloglou C, Mooi WJ, Peeper DS. The essence of senescence. Genes Dev. 2010; 24:2463–2479. [PubMed: 21078816]
26. Herzog B, Pellet-Many C, Britton G, Hartzoulakis B, Zachary IC. VEGF binding to NRP1 is essential for VEGF stimulation of endothelial cell migration, complex formation between NRP1 and VEGFR2, and signaling via FAK Tyr407 phosphorylation. Mol. Biol. Cell. 2011; 22:2766–2776. [PubMed: 21653826]

27. Pan Q, et al. Blocking neuropilin-1 function has an additive effect with anti-VEGF to inhibit tumor growth. Cancer Cell. 2007; 11:53–67. [PubMed: 17222790]

28. Uniewicz KA, Cross MJ, Fernig DG. Exogenous recombinant dimeric neuropilin-1 is sufficient to drive angiogenesis. J. Biol. Chem. 2011; 286:12–23. [PubMed: 20956519]

29. Lippmann ES, et al. Derivation of blood-brain barrier endothelial cells from human pluripotent stem cells. Nat. Biotechnol. 2012; 30:783–791. [PubMed: 22729031]

30. Lee MR, et al. Epigenetic regulation of NANOG by miR-302 cluster-MBD2 completes induced pluripotent stem cell reprogramming. Stem Cells. 2013; 31:666–681. [PubMed: 23255147]

31. Broxmeyer HE, et al. Hematopoietic stem/progenitor cells, generation of induced pluripotent stem cells, and isolation of endothelial progenitors from 21- to 23.5-year cryopreserved cord blood. Blood. 2011; 117:4773–4777. [PubMed: 21393480]

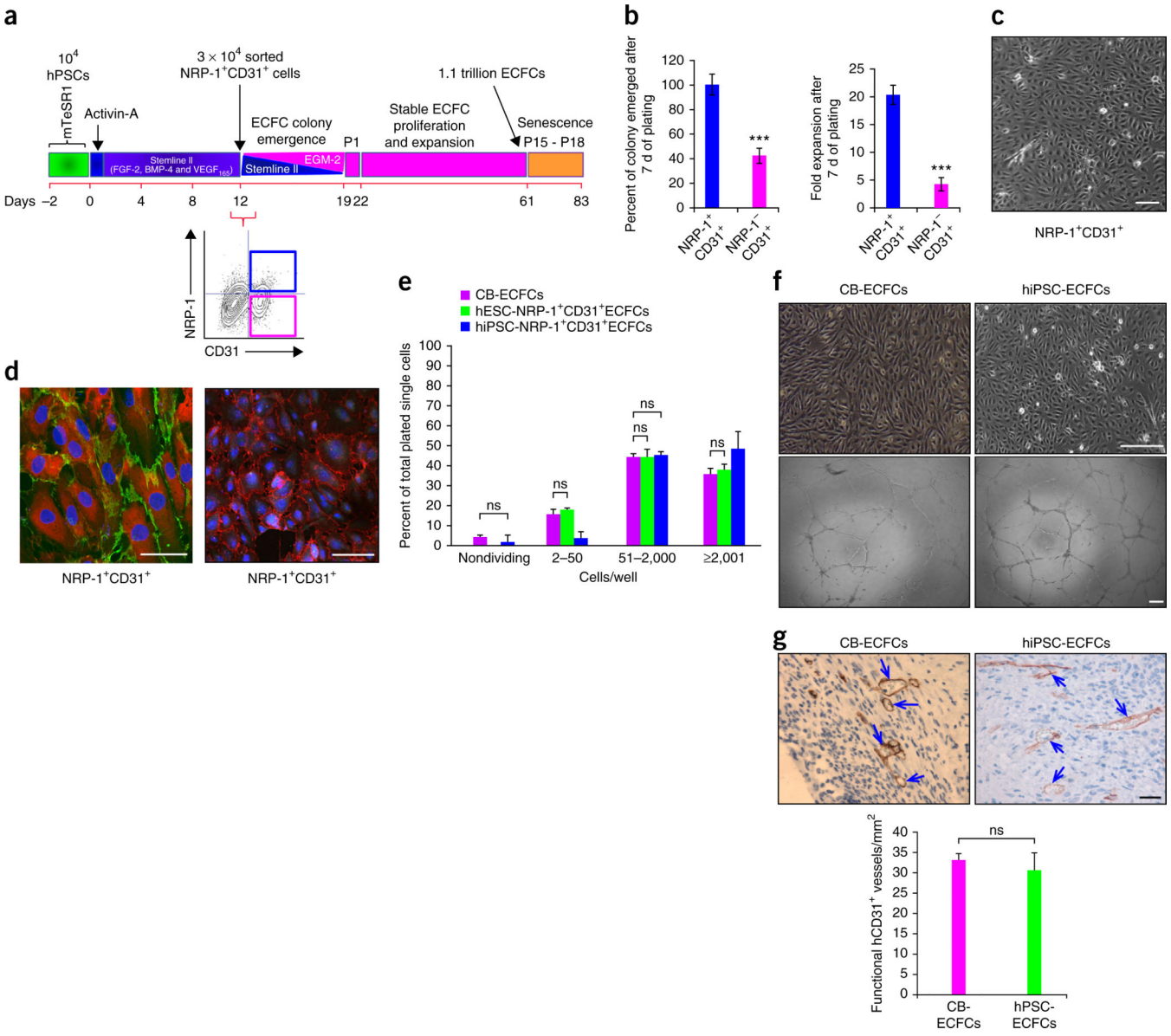

Figure 1.

Simple one-step, 2D, serum-free, endothelial lineage differentiation protocol does not require embryoid body formation or TGF-β inhibition and yields ECFCs similar to those found in cord blood. (**a**) Schematic representation showing an estimation of generation of over a trillion cells in 61 d, starting from 10^4 hESCs or hiPSCs. Generation of 3×10^4 NRP-1$^+$CD31$^+$ cells in 12 d is shown on left. A representative flow cytometry contour plot (bottom right) indicates the percent expression of NRP-1 and CD31 in day 12 differentiated cells. Day 12 NRP-1$^+$CD31$^+$ cells give rise to stable ECFC colonies that undergo extensive expansion. (**b**) Day 12 differentiated cells were sorted for NRP-1$^+$CD31$^+$ and NRP-1$^-$CD31$^+$ cell fractions and cultured in transitioning media for endothelial growth. NRP-1$^+$CD31$^+$ cells gave rise to 60% more endothelial colonies (left panel) and 15-fold more total endothelial cells (right panel) compared to NRP-1$^-$CD31$^+$ cells in 7 d of culture. $n = 5$; mean ± s.d. Student's *t*-test: ***$P < 0.001$. (**c**) A representative photomicrograph of

ECFC colony obtained from NRP-1^{+}CD31^{+} cell fraction exhibiting characteristic cobblestone morphology containing homogenous population of endothelial cells within each colony. Experiments were performed eight times in duplicate. Scale bars, 50 μm. (**d**) Representative immunofluorescence micrographs of ECFCs exhibiting cell surface expression for typical endothelial markers CD31, CD144 and NRP-1 and the nonendothelial marker α-SMA. Left, NRP-1 expression (red); CD31 (green). Right, α-SMA (green); CD144 (red). Nucleus (DAPI, blue). All experiments were performed three times in duplicate. Scale bars, 50 μm. (**e**) Clonal proliferative analysis of hESC-ECFCs and hiPSC-ECFCs in comparison with CB-ECFC control. The distribution pattern of colonies formed by clones of hESC-ECFCs and hiPSC-ECFCs formed HPPs (≥2,001 cells/well) and low PPs (51–2,000 cells/well) similar to levels produced by CB-ECFCs. $n = 3$; mean ± s.d. Student's *t*-test: *P* value not significant (ns). (**f**) Representative phase-contrast photomicrographs of hiPSC-ECFCs' characteristic cobblestone morphology and formation of complete capillary networks on Matrigel similar to that exhibited by CB-ECFCs. All experiments were performed five times in duplicate. Scale bars, 100 μm. (**g**) ECFCs form durable and functional *in vivo* human vessels in immunodeficient mice. ECFCs (both from cord blood and hiPSCs) containing cellularized collagen gels were implanted in immunodeficient (NOD/SCID) mice in a subcutaneous pouch, recovered 14 d later, and fixed and stained. Arrows in the representative photomicrograph depict anti-human CD31^{+}-stained functional human blood vessels that are perfused with circulating host mouse red blood cells. Scale bar, 50 μm. A bar graph represents quantification of functional hCD31^{+} vessels counted per mm^{2} in each group. $n = 3$; mean ± s.d. Student's *t*-test: ns.

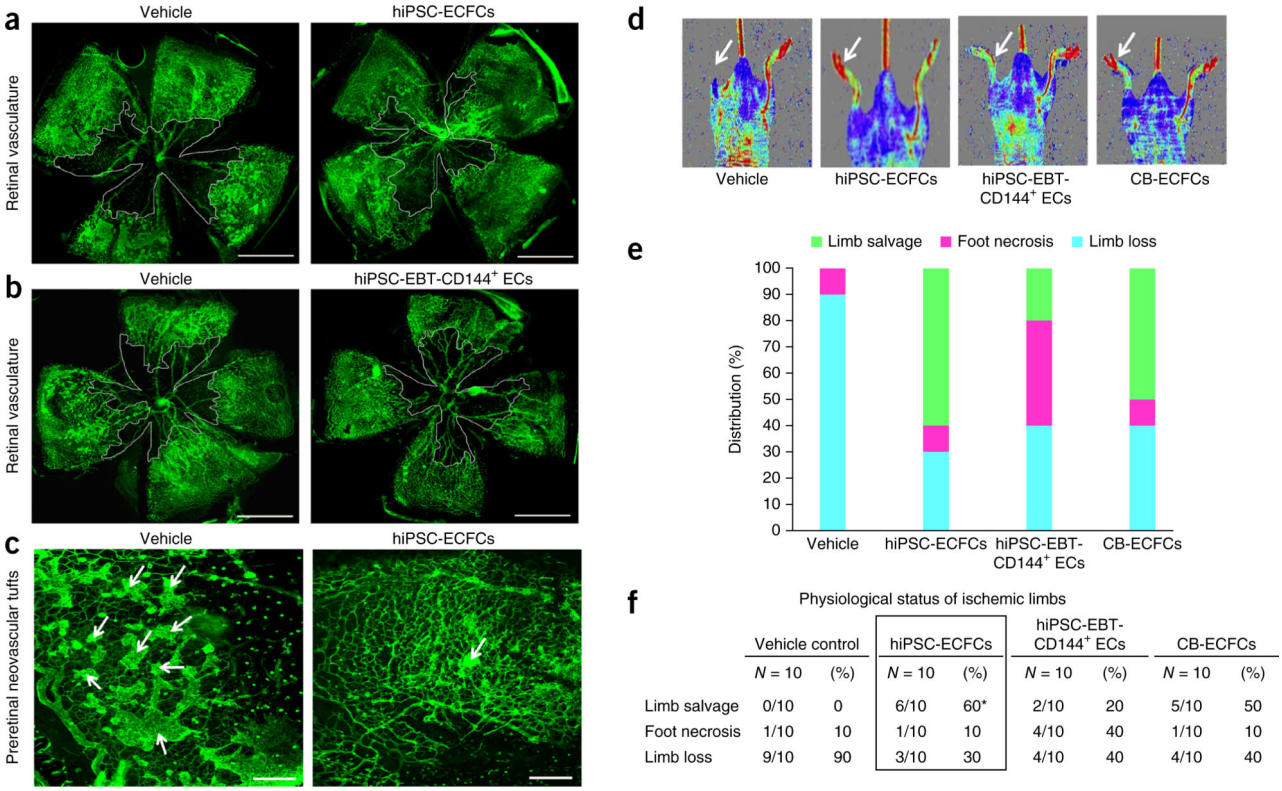

f

Physiological status of ischemic limbs

	Vehicle control		hiPSC-ECFCs		hiPSC-EBT-CD144$^+$ ECs		CB-ECFCs	
	N = 10	(%)	*N* = 10	(%)	*N* = 10	(%)	*N* = 10	(%)
Limb salvage	0/10	0	6/10	60*	2/10	20	5/10	50
Foot necrosis	1/10	10	1/10	10	4/10	40	1/10	10
Limb loss	9/10	90	3/10	30	4/10	40	4/10	40

Figure 2.

Human iPSC-ECFCs contribute to vascular repair of both ischemic retina and limb. (**a**) Representative flat-mounted retinas of C57/BL6 mice injected with vehicle (left) or hiPSC-ECFCs (right). Retinal vasculature stained in green with Isolectin B4. Avascular area indicated by white line. All experiments were performed ≥4 times and percentage of avascular area calculated. Scale bars, 1 mm. (**b**) Representative flat-mounted retinas of C57/BL6 mice injected with vehicle (left) or hiPSC-EBT-CD144$^+$ ECs (right). Retinal vasculature stained in green with Isolectin B4. Avascular area indicated by white line. All experiments were performed ≥4 times and percentage of avascular area calculated. Scale bars, 1 mm. (**c**) Representative pathological preretinal neovascularisation in C57/BL6 mice injected with vehicle (left) or hiPSC-ECFCs (right). Preretinal neovascular tufts predominately seen in vehicle-injected eyes when compared to contra lateral hiPSC-ECFCs–injected eyes. Arrows indicate preretinal neovascular tufts. All experiments were performed ≥4 times. Scale bars, 200 μm. (**d**) Representative laser Doppler perfusion imaging showing therapeutic neovascularization by hiPSC-ECFCs in athymic nude mice. A greater increase in limb blood perfusion was observed in the ischemic limbs (arrow) of mice that received hiPSC-ECFCs or CB-ECFCs transplantation than in the vehicle or hiPSC-EBT-CD144$^+$ ECs-injection groups. All experiments were performed ≥10 times. (**e**) A stacked bar graph represents the percentage distribution of the physiological status of the instrumented ischemic limbs on day 28 post-implantation of vehicle, hiPSC-ECFCs, hiPSC-EBT-CD144$^+$ ECs or CB-ECFCs. All experiments were performed ≥10 times. (**f**) A table represents the physiological status of the ischemic limbs on day 28 post-implantation of vehicle, hiPSC-ECFCs, hiPSC-EBT-CD144$^+$ ECs or CB-ECFCs. All experiments were performed ≥10

times and values represent percentage limb salvage, necrosis or loss. Parametric Chi-squared test: *$P < 0.05$.

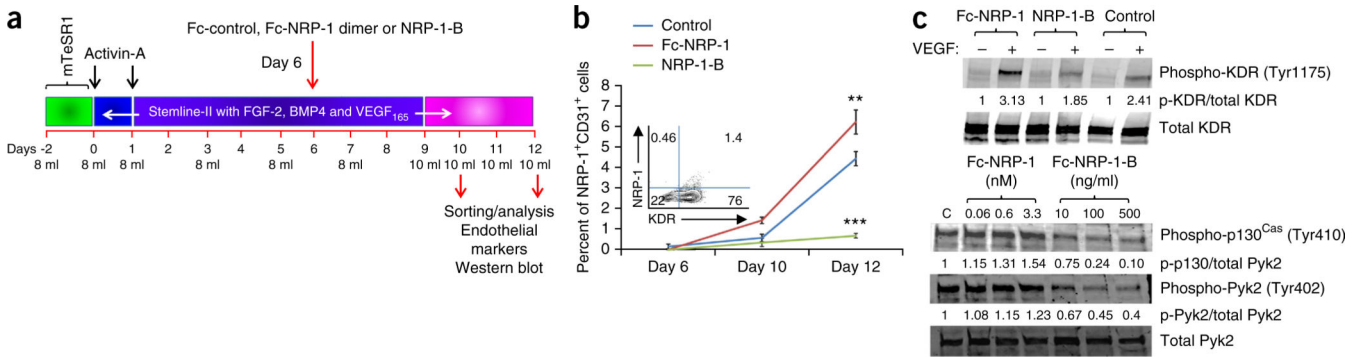

Figure 3.

NRP-1 is critical for the emergence of ECFCs from hPSCs. (**a**) Schematic representation of the treatment strategy in examining the role of NRP-1 in the emergence of ECFCs from hPSCs. (**b**) Quantification of the percentage emergence of NRP-$1^{+}$$CD31^{+}$ (double)- positive cells following treatments with control (blue), Fc-NRP-1 (brown) and NRP-1-B (green) on days 10 and 12 of differentiation. A significantly increased percent emergence of double-positive cells was observed in the Fc-NRP-1–treated group compared to the control group. However, generation of double-positive cells was significantly lower in the NRP-1-B–treated group compared to the control. In the inset, a flow cytometry contour plot indicates the percent expression of KDR and NRP-1 in day 6 differentiated cells showing abundant KDR expression and diminished NRP-1 expression. $n = 3$; mean ± s.d. Student's t-test: $^{**}P < 0.01$ and $^{***}P < 0.001$. (c) Western blots showing KDR, $p130^{Cas}$ and Pyk2 phosphorylation. Top, hPSCs undergoing ECFC differentiation were treated with Fc-control, Fc-NRP-1 dimer or NRP-1-B as described in a, starved, then stimulated with $VEGF_{165}$. Cell lysates were treated with antibodies against phospho-KDR and total KDR. The expression of phosphor-KDR in NRP-1 dimer– and NRP-1-B–treated hiPSCs is shown in top blot and total KDR levels for each lane is depicted in the bottom blot. KDR phosphorylation was observed in VEGF-stimulated groups, and Fc-NRP-1 dimer treatment increased phosphorylation of KDR compared to control-treated cells. However, lower phosphorylation was observed in NRP-1-B–treated cells. Average band intensity value was normalized to total protein for each of the bands, and the normalized band intensity for each group compared with the VEGF-untreated group. In the bottom panels, hiPSCs undergoing ECFC differentiation were treated with the indicated concentration of Fc-control (C), Fc-NRP-1 dimer or NRP-1-B, starved, then stimulated with $VEGF_{165}$. Cell lysates were treated with antibodies against phospho-$p130^{Cas}$, phospho-Pyk2 and total Pyk2 and run on a western blot. Increased P-130^{Cas} and Pyk2 phosphorylation was observed in a dose-dependent manner in the Fc-NRP-1 dimer–treated group compared to control-treated cells. However, lower P-130^{Cas} and Pyk2 phosphorylation was observed in NRP-1-B–treated cells compared to control-treated cells. Average band intensity value was normalized to total protein for each of the bands and the normalized band intensity for each group compared with the band intensity for the control. All experiments were performed three times and representative cropped photomicrographs are shown with quantification of the band intensity at the bottom of each blot. Full-length blots are presented in Supplementary Figure 9.

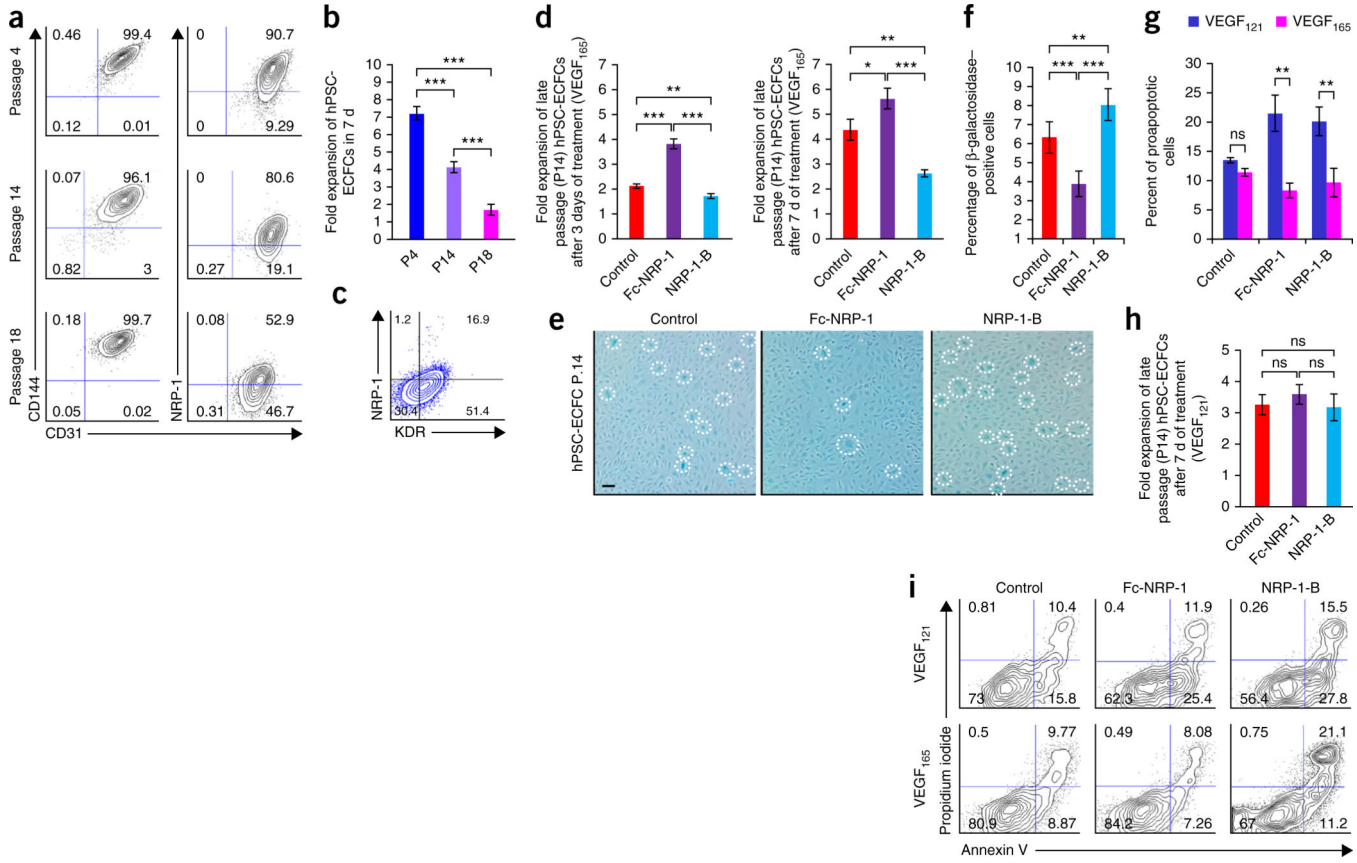

Figure 4.

NRP-1 is critical for the maintenance of ECFC proliferative potential. (**a**) Human PSC-ECFCs from different passages (P4, P14 and P18) were stained with monoclonal antibodies against CD31, CD144 and NRP-1. Percentages in each contour plot indicates CD31 and CD144 double-positive cells (left panel), whereas percentages in the right panel contour plot indicates CD31 and NRP-1 double-positive cells. The percentage of CD31/CD144 double-positive cells was maintained at higher levels in all of these different passages, whereas the percentage of NRP-1/CD31 double-positive cells progressively decreased in late passages. All experiments were performed four times in duplicate and a representative contour plot is shown for each group. (**b**) Fold expansion of hPSC-ECFCs when cells were counted at different passages (P4, P14 and P18) after 7 d of culture. Progressive loss in fold-expansion ability was observed in late-passage cells. $n = 4$; mean ± s.d. Student's t-test: $^{***}P < 0.001$. (**c**) P14 hPSC-ECFCs were stained with monoclonal antibodies against KDR and NRP-1. Percentages in each contour plot indicate NRP-1– and KDR-positive cells. Although more than 50% of the cells exhibited KDR expression, fewer than 17% cells exhibited NRP-1 expression. All experiments were performed four times in duplicate and a representative contour plot is shown. (**d**) Late passage (P14) hPSC-ECFCs were treated with control, Fc-NRP-1 and NRP-1-B to examine fold expansion after 3 or 7 d of treatment. A bar graph represents fold expansion of late passage (P14) hPSC-ECFCs following 3 (left bar graph) and 7 d (right bar graph) of treatment with control, Fc-NRP-1 and NRP-1-B. A significantly increased fold expansion was observed in Fc-NRP-1–treated cells both at day 3 and day 7

compared to control. However, a significantly decreased cell expansion was observed in the NRP-1-B–treated group both at day 3 and day 7 compared to control. $n \geq 3$; mean ± s.d. Student's *t*-test: $^{*}P < 0.05$, $^{**}P < 0.01$ and $^{***}P < 0.001$. (**e**) Late passage (P14) hPSC-ECFCs were treated with control, Fc-NRP-1 and NRP-1-B for 7 d and were stained with β-galactosidase as per manufacturer's instruction. Fc-NRP-1 treatment decreased the number of β-galactosidase–positive blue cells (dotted circles) compared to control-treated cells. Whereas, NRP-1-B treatment increased the number of blue cells compared to control. All experiments were performed 4 times in triplicate and a representative photomicrograph is shown for each group. Scale bar, 50 μm. (f) Percentages of β-galactosidase–positive blue cells following the treatment of late passage (14) hPSC-ECFCs with control, Fc-NRP-1 and NRP-1-B for 7 d. A significantly decreased percentage of blue cells were observed in the Fc-NRP-1–treated group compared to control group. However, a significantly increased percentage of blue cells were observed in the NRP-1-B–treated group compared to control. $n = 6$; mean ± s.d. Student's *t*-test: $^{**}P < 0.01$ and $^{***}P < 0.001$. (**g**) Late passage (p14) hPSC-ECFCs were cultured in regular EGM-2 media containing $VEGF_{165}$ and EGM-2 media with $VEGF_{121}$ and these cells were treated with control, Fc-NRP-1 and NRP-1-B for 7 d. After 7 d cells were collected, counted and stained with propidium iodide and annexin V to examine for live, proapoptotic, and dead cells in each of these treatment groups. A bar graph represents the percentage of proapoptotic cells in $VEGF_{165}$ and $VEGF_{121}$ containing media following 7 d of treatment with control, Fc-NRP-1 and NRP-1-B. A significantly decreased percentage of pro-apoptotic cells were observed in both Fc-NRP-1 and NRP-1-B treated groups in cells cultured in $VEGF_{165}$ containing media compared to cells cultured in the presence of $VEGF_{121}$. $n \geq 3$; mean ± s.d. Student's *t*-test: $^{**}P < 0.01$. (**h**) Late passage (P14) hPSC-ECFCs were cultured in EGM-2 media where regular $VEGF_{165}$ was replaced with $VEGF_{121}$ and these cells were treated with control, Fc-NRP-1 and NRP-1-B for 7 d. A bar graph represents fold expansion of late passage (14) hiPSC-ECFCs in $VEGF_{121}$ treated media following 7 d of treatment with control, Fc-NRP-1 and NRP-1-B. Fc-NRP-1 and NRP-1-B treatment did not cause significant alteration in fold expansion in these cells compared to control in the presence of $VEGF_{121}$. $n = 4$; mean ± s.d. Student's *t*-test; ns. (**i**) Late passage (p14) hPSC-ECFCs were cultured in regular EGM-2 media containing $VEGF_{165}$ and EGM-2 media with $VEGF_{121}$ and these cells were treated with control, Fc-NRP-1 and NRP-1-B for 7 d. After 7 d, cells were collected, counted and stained with propidium iodide and annexin V to examine for live, proapoptotic and dead cells in each of these treatment groups. Percentages in each contour plots represent live, proapoptotic and dead cells in control (left panels), Fc-NRP-1– (middle panels) and NRP-1-B– (right panels) treated cells in the presence of $VEGF_{121}$ (panels on top row) or $VEGF_{165}$ (panels on bottom row). In the $VEGF_{121}$-treated cells, both Fc-NRP-1 and NRP-1-B increased the percentage of dead and pro-apoptotic cells compared to control. However, in $VEGF_{165}$-treated cells, while Fc-NRP-1 decreased the percentages of both dead and proapoptotic cells and increased the percentage of live cells compared to control, NRP-1-B increased the percentages of both dead and proapoptotic cells and decreased the percentage of live cells compared to control. All experiments were performed four times in triplicate and a representative contour plot is shown for each group.